**Proceedings of the 31st International Conference on Ocean, Offshore and Arctic Engineering OMAE2012 June 10-15, 2012, Rio de Janeiro, Brazil**

# OMAE2012-83744

# DRAFT: APPLICATION OF AN ABSORBING BOUNDARY CONDITION IN A WAVE-STRUCTURE INTERACTION PROBLEM

**Bulent Duz***
Department of Ship Hydrodynamics
Technical University of Delft
Mekelweg 2, 2628 CD Delft
The Netherlands
b.duz@tudelft.nl

**Rene H.M. Huijsmans**
Department of Ship Hydrodynamics
Technical University of Delft
Mekelweg 2, 2628 CD Delft
The Netherlands
r.h.m.huijsmans@tudelft.nl

**Peter R. Wellens**
**Mart J.A. Borsboom**
Deltares
P.O. Box 177, 2600 MH Delft
The Netherlands
{peter.wellens, mart.borsboom}@deltares.nl

**Arthur E.P. Veldman**
Institute for Mathematics and Computer Science
University of Groningen
P.O. Box 407, 9700 AK Groningen
The Netherlands
a.e.p.veldman@rug.nl

## ABSTRACT

*For the design of offshore structures, an accurate assessment of the ability of the structure to survive in extreme sea conditions is of prime importance. Next to scaled model tests on the structure in waves, also CFD capabilities are at the disposal of the designer. However even with the fastest computers available, it is still a challenge to use CFD in the design stage because of the large computational resources they require.*

*In this study we focus our attention on the implementation of an absorbing boundary condition (ABC) in a wave-structure interaction problem. Unlike the traditional approach where the boundaries are located far from the object to avoid reflection, we gradually locate them closer while at the same time observing the influence of the absorbing boundary condition on the solution. Numerical calculations are performed using the CFD simulation tool ComFLOW which is a volume-of-fluid (VOF) based Navier-Stokes solver. Comparisons with experimental results are also provided and the performance of the ABC is discussed.*

## INTRODUCTION

Scientists and engineers regard the surface of the ocean as interesting due to one of the broadest physical phenomena which has been intensively studied in various fields of science: waves. Although waves can occur in all types amongst a variety depending on the forces acting on the water, one aspect exists in all the cases and attracts our attention: waves exert loads and stresses on numerous kinds of man-made structures in the ocean. If the other elements of the environment are also hostile, major catastrophic failures can appear threatening human safety and causing economic loss.

Although highly capable numerical features are at the disposal of researchers, particular aspects of numerically solving wave-structure interaction problems in unbounded domains cause various bottlenecks. Typically the phenomena of interest are local but embedded in a vast spatial domain. At this point, the infinite domain, although sometimes it may not be truly unbounded, is truncated via artificial boundaries, thus introducing a finite computational domain and a residual infinite domain. One

*Address all correspondence to this author.

of such bottlenecks is developing a robust and efficient boundary condition to be imposed on these artificial boundaries.

The Sommerfeld boundary condition [1] was the cornerstone of non-reflecting boundary conditions. Engquist and Majda [2] presented a method to develop the first hierarchy of absorbing boundary conditions. Higdon [3] generalized this theory and showed that Engquist and Majda boundary condition is a subset of the Higdon operators. Since high order boundary operators include high order derivatives both in time and space, Collino and Joly [4] introduced the use of auxiliary variables to circumvent this difficulty. This idea has found widespread interest and has been used by Grote and Keller [5], Givoli and Neta [6], and Hagstrom and Warburton [7] among others. For a general review regarding high order local non-reflecting boundary conditions, see [8].

In this paper, we study application of an absorbing boundary condition (ABC) in a wave-structure interaction problem where a fifth-order Stokes wave is traveling under an angle of incidence in a three-dimensional computational domain. Numerical computations are carried out using ComFLOW [9,10]. Here we focus our attention specifically on the performance of the ABC for the duration of the simulations. For this purpose, numerical results are compared to the experimental results. We end the paper with some concluding remarks.

## MATHEMATICAL MODELING

If we consider water as a homogeneous, incompressible, viscous fluid, we can describe fluid motion in a three-dimensional domain $\Omega$ (see Fig. 1) by the continuity equation and the Navier-Stokes equations in a conservative form as,

$$\oint_{\Gamma} \mathbf{u}.\mathbf{n}\, d\Gamma = 0, \tag{1}$$

$$\oint_{\Omega} \frac{\partial \mathbf{u}}{\partial t} d\Omega + \oint_{\Gamma} \mathbf{u}\mathbf{u}^T.\mathbf{n} d\Gamma = -\frac{1}{\rho}\oint_{\Gamma} (p\mathbf{n} - \mu\nabla\mathbf{u}.\mathbf{n}) d\Gamma + \oint_{\Omega} \mathbf{F} d\Omega\,. \tag{2}$$

In Eqns. (1) and (2), $\Omega$ denotes a volume with boundary $\Gamma$ and normal vector $\mathbf{n}$, $\mathbf{u} = (u,v,w)^T$ is the flow velocity, $\rho$ is the fluid density, $p$ is the pressure, $\mu$ is the dynamic viscosity, $\nabla$ is the gradient operator and $\mathbf{F} = (F_x, F_y, F_z)^T$ represents external body forces acting on the fluid such as gravity. For discretization of Eqns. (1) and (2), see, e.g., [11, 12].

To solve Eqns. (1) and (2) in $\Omega$, we impose three types of boundary conditions: the Dirichlet boundary, the generating and absorbing boundary and a free surface conditions. Below we describe these boundary conditions.

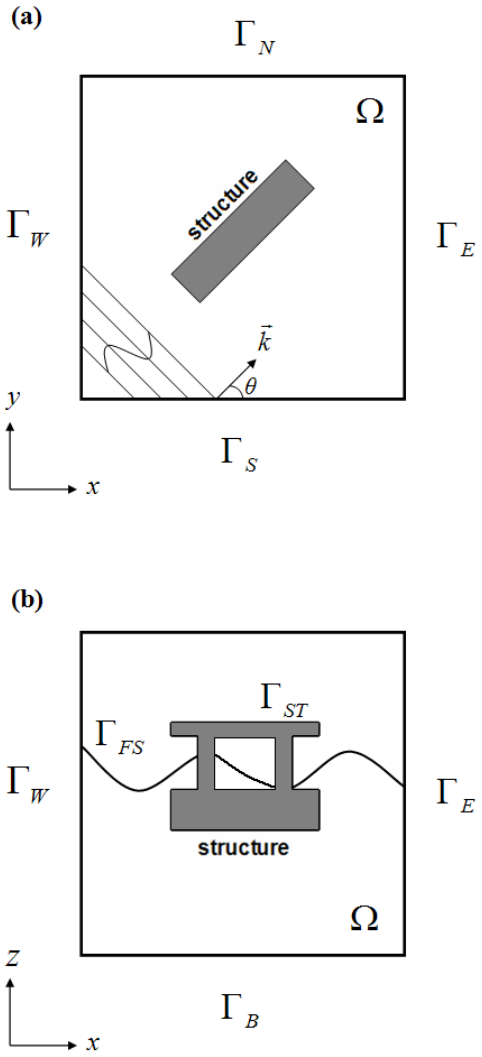


**FIGURE 1**. A COMPUTATIONAL DOMAIN WITH A STRUCTURE LOCATED AT THE CENTER. $\Gamma_N$, $\Gamma_E$, $\Gamma_S$ and $\Gamma_W$ ARE ARTIFICIAL BOUNDARIES ON WHICH AN ABC IS TO BE APPLIED.

***On the north and east boundaries*** $\Gamma_N$ ***and*** $\Gamma_E$:
On the north and east boundaries $\Gamma_N$ and $\Gamma_E$ the absorbing boundary condition (ABC) is prescribed. The boundary condition on $\Gamma_N$ and $\Gamma_E$ should allow the waves to move out of the computational domain without generating spurious reflection. Here, we will derive this boundary condition only for $\Gamma_E$ since it is rather straightforward to extend the idea to $\Gamma_N$. Now, consider the following boundary operator:

$$\left(\cos\alpha\frac{\partial}{\partial t} + c^{out}\frac{\partial}{\partial x}\right)\Phi^{out} = 0\,. \tag{3}$$

Equation (3) is perfectly absorbing if the boundary parameter $\alpha$ is equal to the angle of incidence $\theta$ of a wave (see Fig. 1(a)) characterized by the velocity or wave potential $\Phi^{out}$ and traveling out of the domain with the phase speed $c^{out}$. To make Eqn. (3) independent of the phase speed $c^{out}$, we introduce the following rational expression which approximates the dispersion relation,

$$c^{out} \approx \sqrt{gh}\frac{a_0 + a_1(k^{out}h)^2}{1 + b_1(k^{out}h)^2} , \tag{4}$$

where a proper choice of coefficients $a_0$, $a_1$ and $b_1$ leads to a close approximation for the largest possible range of $k^{out}h$ values. Thus, reflection from the boundary will be minimized over that specific range. Next, exploiting the exponential behavior of $\Phi^{out}$ in the $z$ direction, we can replace the wave number $k^{out}$ with

$$k^2\Phi^{out} = \frac{\partial^2}{\partial z^2}\Phi^{out} . \tag{5}$$

By means of Eqns. (4) and (5), the wave number is resolved using the velocity potential $\Phi^{out}$.

Since Eqns. (1) and (2) are specified as the governing equations, the time and spatial derivatives of the velocity potential in Eqn. (3) must be interpreted in terms of the velocity components and pressure. Recalling the linearized Bernoulli equation and potential theory, we have $\partial\Phi/\partial t = -p_b - gz_p$ and $\partial\Phi/\partial x = u_b$. Finally, combining Eqns. (3), (4) and (5), we obtain

$$\begin{aligned}&\cos\alpha\left(1 + b_1h^2\frac{\partial^2}{\partial z^2}\right)p_b \\ &-\sqrt{gh}\left(a_0 + a_1h^2\frac{\partial^2}{\partial z^2}\right)u_b + gz_p = 0 .\end{aligned} \tag{6}$$

In Eqn. (6) the subscript $b$ indicates that the quantity is defined at the boundary and the subscript $p$ indicates that the quantity is evaluated at the elevation of the pressure point. For the discrete form of the ABC, see [13].

***At the free surface*** $\Gamma_{FS}$:
At the free surface $\Gamma_{FS}$ resulting from the continuity of normal and tangential stresses the following conditions are implemented for the velocity components and the pressure,

$$\mu\left(\frac{\partial u_n}{\partial t} + \frac{\partial u_t}{\partial n}\right) = 0 , \tag{7}$$

$$-p + 2\mu\frac{\partial u_n}{\partial n} = -p_0 + \sigma\kappa , \tag{8}$$

where $u_n$ and $u_t$ correspond to the normal and tangential component of the velocity, respectively, $p_0$ is the atmospheric pressure, $\sigma$ is the surface tension and $\kappa$ is the total curvature of the free surface. If we describe the position of the free surface by $s(\mathbf{x},t) = 0$, the displacement of the free surface can be computed via,

$$\frac{Ds}{Dt} = \frac{\partial s}{\partial t} + (\mathbf{u}.\nabla)s = 0 . \tag{9}$$

For the reconstruction and advection of the free surface, see, e.g., [14, 15].

***On the bottom and structure*** $\Gamma_B$ ***and*** $\Gamma_{ST}$:
On the bottom and structure $\Gamma_B$ and $\Gamma_{ST}$ we specify a no-slip no-penetration condition which is simply the Dirichlet condition, i.e. $\mathbf{u} = 0$.

***On the west and south boundaries*** $\Gamma_W$ ***and*** $\Gamma_S$:
On the west and south boundaries $\Gamma_W$ and $\Gamma_S$ the generating and absorbing boundary condition (GABC) is applied. The GABC should play the role of an open boundary condition permitting waves to move into and out of the computational domain. When the total wave signal at the inflow boundary is decomposed as $\Phi = \Phi^{in} + \Phi^{out}$, then it is straightforward to substitute this relation in Eqn. (3). Here, $\Phi^{in}$ represents the incoming wave which is known beforehand and given in Tab. 1(a) whereas $\Phi^{out}$ represents the outgoing wave which is diffracted from the structure and propagating in all directions. For the discrete form of the GABC, see [16].

By means of all the boundary conditions explained above we complete the statement of the problem.

## NUMERICAL SIMULATION

We apply the mathematical model, expressed in the previous section, to a problem in three dimensions where a fifth-order Stokes wave is traveling under an angle of incidence in a computational domain with a structure located at the center (see Fig. 1 for an illustration of the problem). The structure is a semi-submersible consisting of two columns and a pontoon under water, see Fig. 5(a) for the dimensions of the semi-submersible at full scale. Now, we define a parameter $d$ which controls the dimensions of the computational domain on the $x-y$ plane as shown in Fig. 2. Basically, we choose two values for $d$: $d = 1L = 130m$ and $d = 0.5L = 65m$ where $L$ denotes the wave length. The first choice results in a domain with the length and width of $R_x = R_y = 265m$ whereas in the second case the length and width are $R_x = R_y = 173m$. Table 1(b) gives configurations of the test cases. As we locate the boundaries closer to the structure, we will investigate how the GABC influences the results. Note that in both of the cases, the dimension of the computational domain in the $z$ direction is $R_z = 210m$ and the water depth is $h = 180m$.

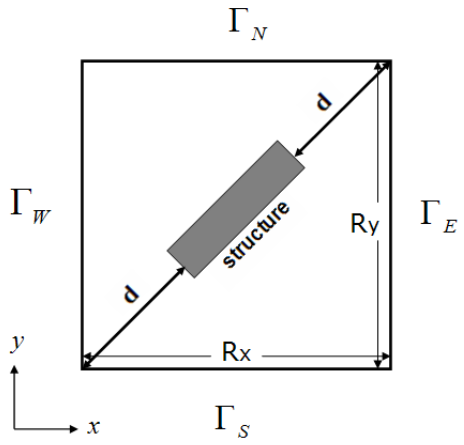


**FIGURE 2**. PARAMETER $d$ CONTROLS THE DIMENSIONS OF THE COMPUTATIONAL DOMAIN ON THE $x-y$ PLANE.

(a) CHARACTERISTICS OF THE WAVE.

| WAVE | 5th-order Stokes wave | | | | |
|---|---|---|---|---|---|
| | period | heigth | length | steepness | water depth |
| | T (s) | H (m) | L (m) | H/L | h (m) |
| W9 | 9 | 7,5 | 130 | 0,058 | 180 |

(b) CONFIGURATIONS OF THE COMPUTATIONAL DOMAIN IN CASE 1 AND CASE 2.

| | Characteristics of the test cases | | | | |
|---|---|---|---|---|---|
| | Distance d (m) | Domain size Rx × Ry × Rz | Number of cells | Boundary condition on $\Gamma_W$ and $\Gamma_S$ | Boundary condition on $\Gamma_N$ and $\Gamma_E$ |
| Case 1 | 1L | 265m×265m×210m | 1.5 million | GABC | ABC |
| Case 2 | 0.5L | 173m×173m×210m | 0.9 million | GABC | ABC |

**TABLE 1**. INPUTS FOR THE NUMERICAL SIMULATIONS.

To capture the details of the flow near the structure, a finely spaced grid in all directions is used as sketched in Fig. 3(a). However, far away from the structure, the grid becomes progressively coarser.

The characteristics of the fifth-order Stokes wave are given in Tab. 1(a). At $t = 0$ this wave is generated and initialized everywhere in the computational domain as depicted in Fig. 3(b). At every time step starting from the initial condition, the solution variables are updated according to the fifth-order Stokes wave theory [17] and prescribed at the inflow boundaries.

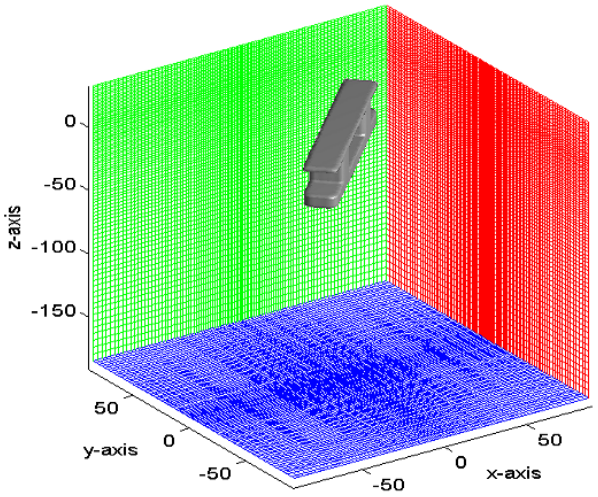


(a) A VIEW OF COMPUTATIONAL GRID.

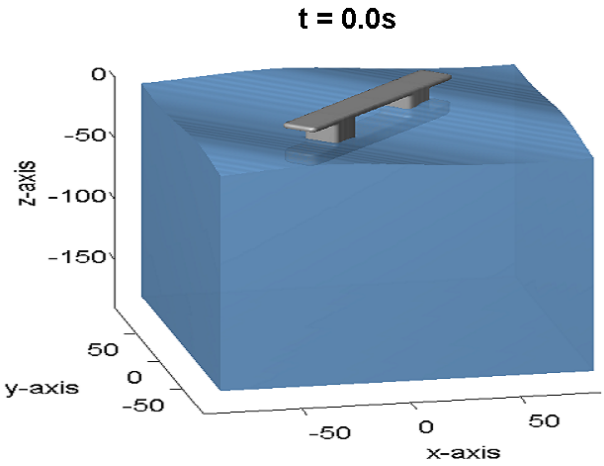


(b) INITIAL CONDITION FOR THE NUMERICAL COMPUTATION. ANGLE OF INCIDENCE IS 45°.

**FIGURE 3**. BASIC SETUP FOR THE SIMULATION IN CASE 2. THE SAME PROCEDURE IS FOLLOWED FOR CASE 1 AS WELL.

## EXPERIMENTAL MODELING

The tests were carried out at Maritime Research Institute (MARIN) in the Netherlands in 2008. Several experimental parameters were specified, such as the design of the semi-submersible and the generated sea states, to provide a comprehensive analysis regarding the physics behind the wave-structure interaction. In this section, we present some details of the test considered in this study. The 1:50 scale of the semi-submersible (see Figs. 4(a) and 4(b) for the photographs of the semi model in the work shop and in the experiment, respectively. Also, see Fig. 5(a) for the general plan of the semi-submersible at full scale) was modeled and its position was fixed in the High Speed

Basin with dimensions 200m long by 4m wide by 4m deep. The basin is equipped with a flap-type wave generator at one end and a beach at the other end. The center of the test set-up was located 100m away from the wave flap. For simplicity, in the remainder of this paper all the details will be presented in prototype values unless stated otherwise.


(a) THE 1:50 MODEL OF THE SEMI-SUBMERSIBLE IN THE WORK SHOP.

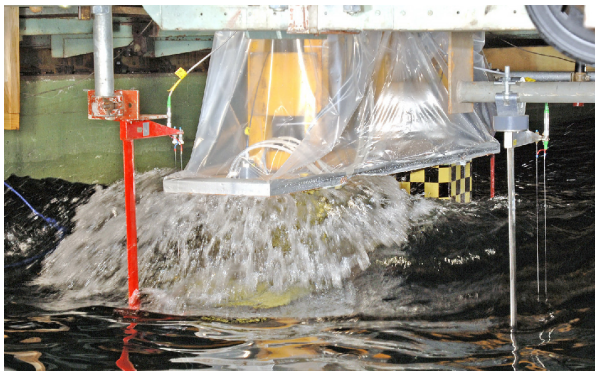

(b) WAVE RUN-UP AND IMPACT ON THE FORWARD COLUMN AND DECK IN REGULAR WAVES.

**FIGURE 4**. PHOTOGRAPHS OF THE SEMI-SUBMERSIBLE MODEL IN THE WORK SHOP AND IN THE EXPERIMENT.

The waves were produced with a flap-type wave generator at one end of the basin. The surface elevations were measured using resistance type wave probes at various locations on and around the model. Additionally, piezo-type pressure transducers were attached to the structure to monitor wave impact pressures for the duration of the tests, see Fig. 5(b) for the positions of the measurement instruments which will be utilized to compare the numerical results to the experimental results. Also, video recordings were made during the model tests using various types of cameras. The measurements ceased as soon as it was obvious that reflected waves from the beach started to arrive at the semi model in the basin.

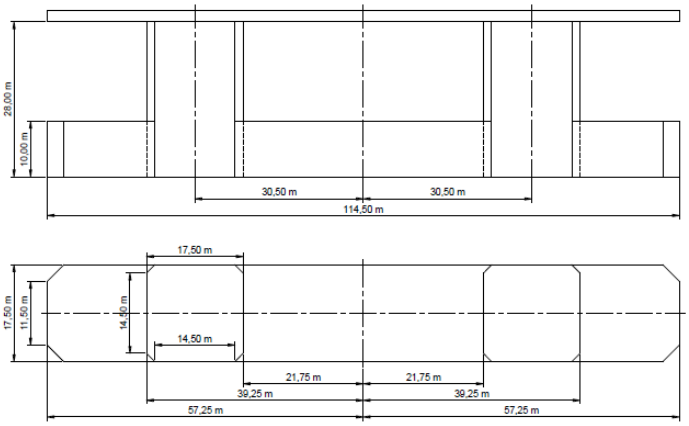


(a) GENERAL PLAN OF THE SEMI-SUBMERSIBLE AT FULL SCALE.

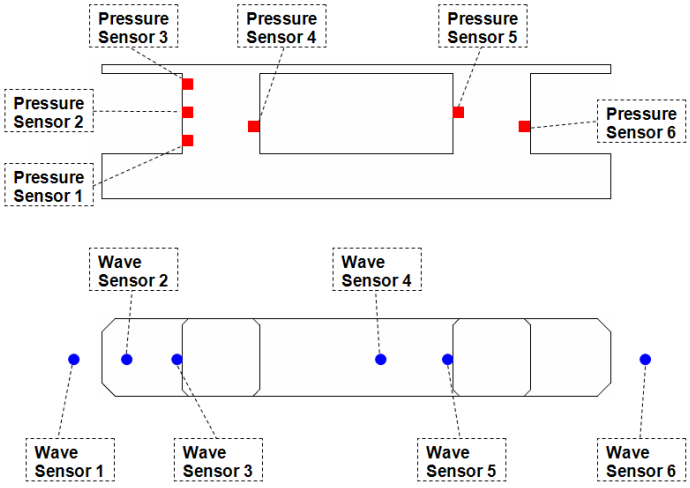


(b) POSITIONS OF THE WAVE PROBES AND PRESSURE TRANSDUCERS.

**FIGURE 5**. DETAILS OF THE SEMI-SUBMERSIBLE AND MEASUREMENT INSTRUMENTS.

Several sea states were generated including regular and irregular long crested head waves. Here, we will present the results for the wave given in Tab. 1(a).

## RESULTS AND DISCUSSION

In this section, we will compare two simulations given in Tab. 1(b) to each other and to the experiment. For this purpose, we will utilize measurements of the wave elevation and wave impact pressures at various positions during the experiment and numerical simulations where the entire structure was restrained.

The duration of the numerical simulations is 40 seconds, which is approximately 4 wave periods. However, the experi-

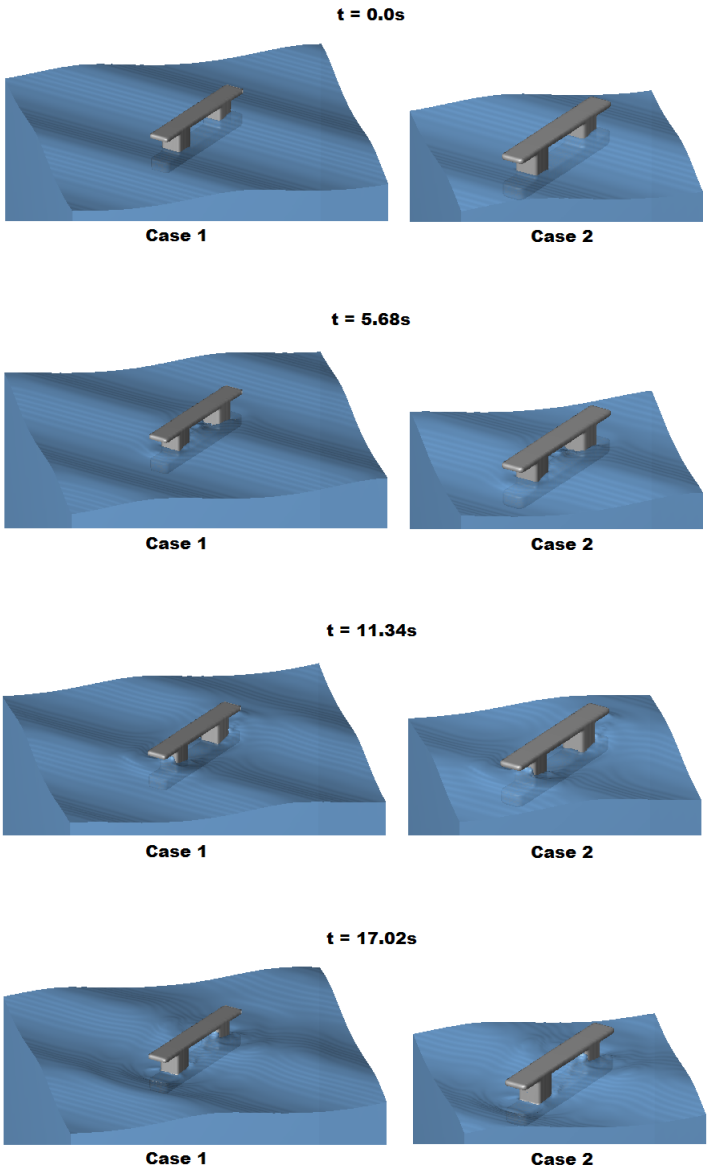


**FIGURE 6**. SNAPSHOTS OF THE NUMERICAL SIMULATIONS IN CASE 1 AND CASE 2 AT VARIOUS INSTANCES IN TIME.

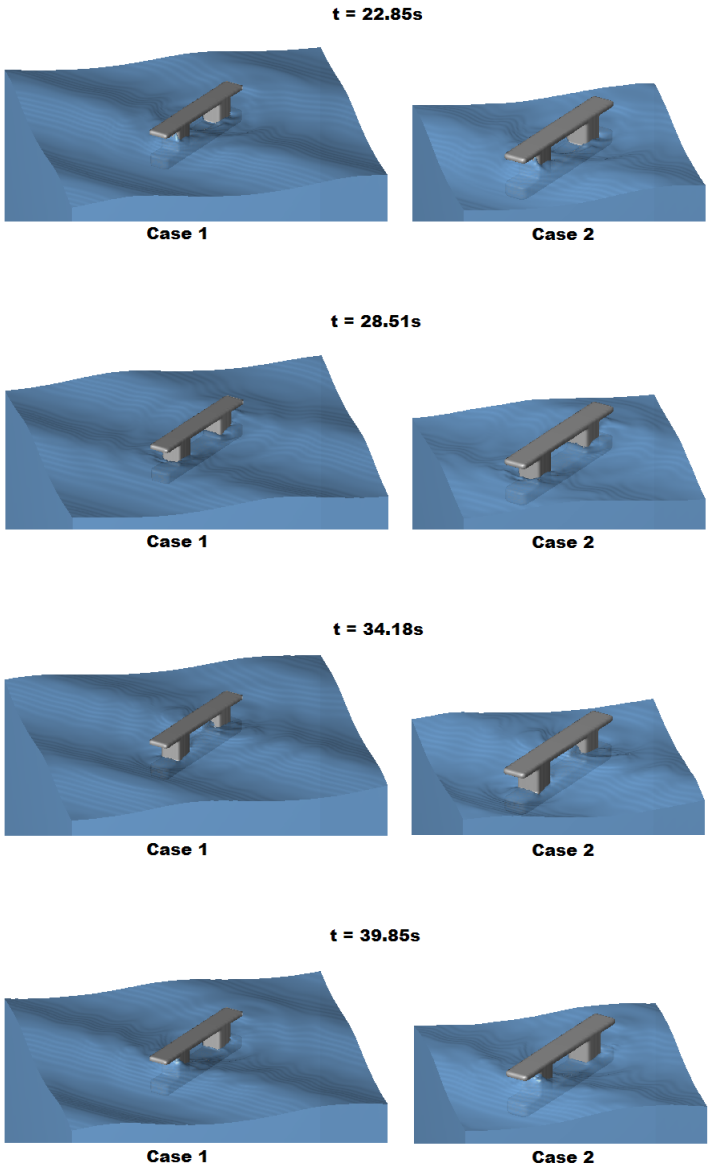


**FIGURE 7**. CONTINUED FROM FIG. 6.

ment continued for 1850 seconds. Therefore, at first, we had to specify a time frame of 40 seconds from the experiment during which the wave field is fully developed but the effect of the side walls and the beach is not dominant. After analyzing time traces of the measured signals, $t = 1105s$ is selected as the starting point and during the subsequent 40 seconds the comparisons are made between the numerical simulations and the experiment.

Two simulations are carried out to investigate the performance of the absorbing boundary condition which is applied on the boundaries surrounding the structure. Table 1(b) gives details of these simulations. The basic difference between Case 1 and Case 2 is the dimensions of the computational domain on the $x-y$ plane. As we locate the boundaries closer to the structure in Case 2, the number of cells used in the simulation reduces substantially, which as a result saves memory consumption as well as computational effort. In this section, we will demonstrate whether this advantage comes at a price.

Figures 6 and 7 show snapshots of the simulations at numerous instances for Case 1 and Case 2. Throughout both of the simulations, we detect no apparent differences at the free surfaces between two computations, which is very much expected.

Figures 8 and 9 show the wave elevation and Figs. 10 and 11 show the wave impact pressure at various locations, see Fig. 5(b)

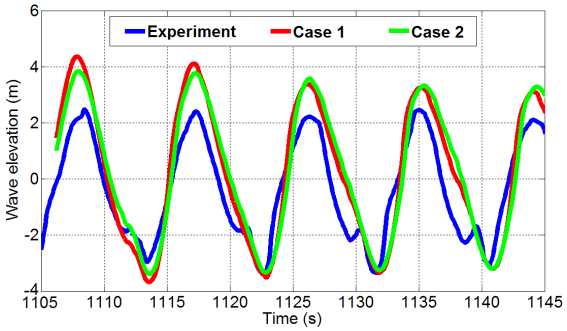


(a) WAVE SENSOR 1

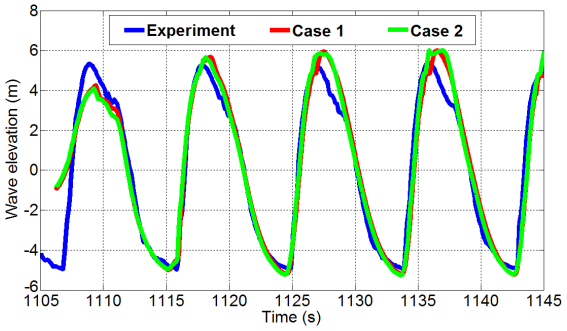


(b) WAVE SENSOR 2

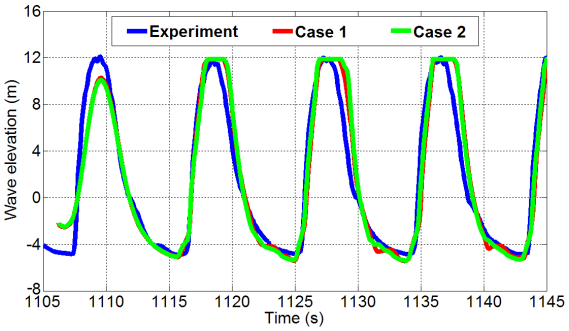


(c) WAVE SENSOR 3

**FIGURE 8**. WAVE ELEVATION AT VARIOUS LOCATIONS.

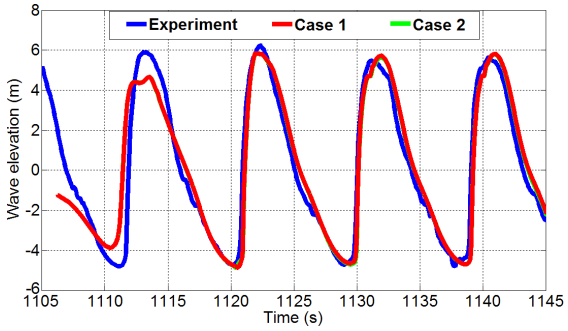


(a) WAVE SENSOR 4

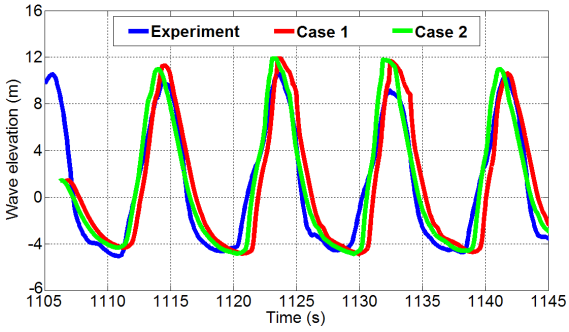


(b) WAVE SENSOR 5

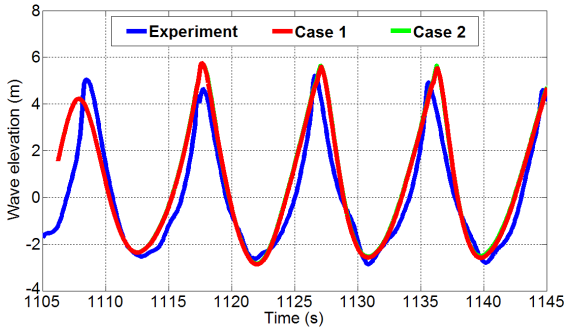


(c) WAVE SENSOR 6

**FIGURE 9**. CONTINUED FROM FIG. 8.

for the positions of the wave probes and pressure transducers. Observing Figs. 8 to 11, we first notice that the results from the numerical simulations agree well with each other although sometimes they do not with the experiment. As a first requirement, we expect the solution in Case 2 to be reasonably close to that in Case 1. Essentially, the procedure of reducing the size of the domain in Case 2 aimed to reduce the computational effort while replicating the solution in Case 1 regardless of how accurate it is. Close examination of the results demonstrate that both the wave elevation and wave impact pressure at numerous positions behave very similarly in Case 1 and Case 2.

The second step is to validate the numerical calculations. Overall, the numerical results are in reasonable agreement with the experimental results. However, we notice relatively large differences between the simulations and the experiment for a short time frame following the starting instant, i.e., $t = 1105s$. As mentioned earlier, the initial condition in the numerical simulations is the fifth-order Stokes wave prescribed throughout the computational domains, see Fig. 6 for an illustration of the initial condition in Case 1 and Case 2. Since the Stokes wave theory does

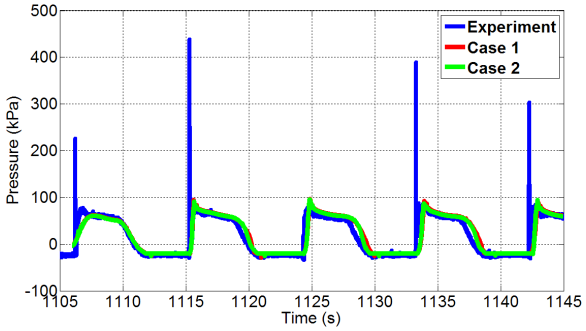


(a) PRESSURE SENSOR 1

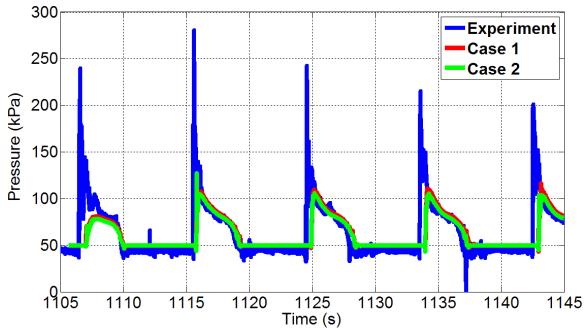


(b) PRESSURE SENSOR 2

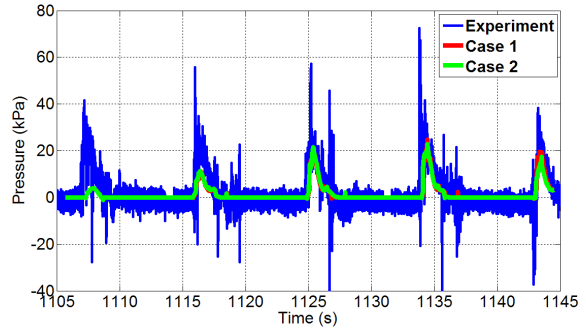


(c) PRESSURE SENSOR 3

**FIGURE 10**. WAVE IMPACT PRESSURE AT VARIOUS LOCATIONS.

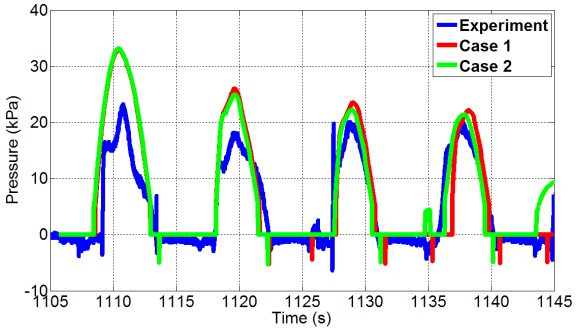


(a) PRESSURE SENSOR 4

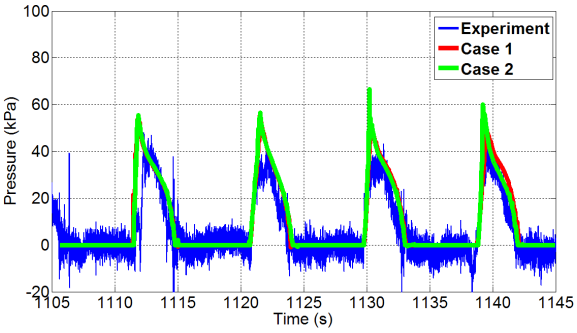


(b) PRESSURE SENSOR 5

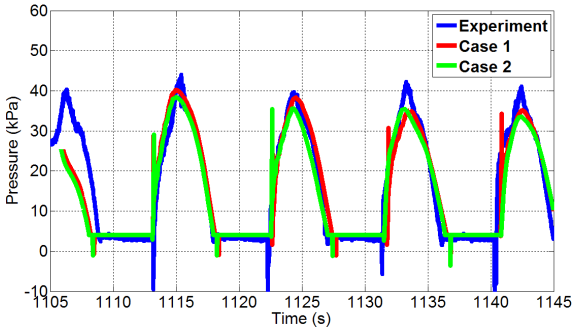


(c) PRESSURE SENSOR 6

**FIGURE 11**. CONTINUED FROM FIG. 10.

not include the effects of diffraction, the initial wave kinematics of the numerical simulations do not have one-to-one correspondence with those of the experiment. As a result, until the diffracted waves from the structure start affecting the flow behavior, high deviations occur in terms of both surface elevation and impact pressure.

Although the absorbing boundary condition performs fairly well, a grid convergence study is needed to provide a comprehensive analysis for error assessment. If we take $f$ as a refinement factor and include time in the refinement as well, we will have a work increase of a factor of $f^4$ between any two levels. Considering the duration and total point counts of the simulations presented in the current work, a grid convergence study causes substantial computational cost. We hope to report about this in a future publication.

## CONCLUSIONS

We have presented numerical and experimental results for a wave-structure interaction problem where one half of a typical

semi-submersible was restrained in a regular head sea. Wave elevation and wave impact pressures were measured at various locations for comparisons.

In the numerical computations, an absorbing boundary condition is incorporated into the CFD simulation tool ComFLOW. The performance of the ABC is assessed by means of the measurements. Throughout the major part of the simulations, numerical results are in reasonable agreement with the experiment. Calculation of the wave elevation and impact pressure exerted by the waves on the structure is not significantly affected by the application of the absorbing boundary condition when the boundaries are located closely to the structure. Consequently, computational costs are reduced considerably without compromising the numerical solution.

## ACKNOWLEDGMENT

The research is supported by the Dutch Technology Foundation STW, applied science division of NWO and the technology programma of the Ministry of Economic Affairs in The Netherlands (contracts GWI.6433 and 10475). The authors kindly thank the Maritime Research Institute in the Netherlands (MARIN) for the experimental results.

## REFERENCES

[1] Sommerfeld, A., 1949. "Partial differential equations in physics". Academic Press.

[2] Engquist, B. and Majda, A., 1977. "Absorbing boundary conditions for the numerical simulation of waves". *Math. Comput.*, **31**, pp. 629-651

[3] Higdon, R. L., 1987. "Numerical absorbing boundary conditions for the wave equation". *Math. Comput.*, **49**, 65-90.

[4] Collino, F. and Joly, P., 1995. "New absorbing boundary conditions for the finite element solution of 3D Maxwell's equations". *IEEE. Transactions on Magnetics*, **31(3)**, 1696-1701.

[5] Grote, M. J. and Keller, J. B. Nonreflecting boundary conditions for time-dependent scattering. *Journal Of Computational Physics* (1996) **127(1)**:52-65.

[6] Givoli, D. and Neta, B. High-order non-reflecting boundary conditions for dispersive waves. *Wave Motion* (2003) **37(3)**:257-271.

[7] Hagstrom, T. and Warburton, T. A new auxiliary variable formulation of high-order local radiation boundary conditions: corner compatibility conditions and extensions to first-order systems. *Wave Motion* (2004) **39(4)**:327-338.

[8] Givoli, D., 2004. "High-order local non-reflecting boundary conditions: a review". *Wave Motion*, **39**, pp. 319-326

[9] Veldman, A.E.P., Luppes, R., Bunnik, T., Huijsmans, R.H.M., Duz, B., Iwanowski, B., Wemmenhove, R., Borsboom, M.J.A., Wellens, P.R., van der Heiden, H.J.L., van der Plas, P., 2011. "Extreme wave impact on offshore platforms and coastal constructions". In Proc. 30th Int. Conf. on Ocean, Offshore and Arctic Engineering OMAE2011. Paper OMAE2011-49488

[10] Luppes, R., Duz, B., van der Heiden, H.J.L., van der Plas, P. and Veldman, A. E. P., 2011. "Numerical simulation of extreme wave impact on offshore platforms and coastal constructions". In Proc. 5th Int. Conf. on Computational Methods in Marine Engineering MARINE2011.

[11] Verstappen, R. W. C. P., Veldman, A. E. P., 2003. "Symmetry-preserving discretization of turbulent flow". *J. Comput. Phys.*, **187**, pp. 343368.

[12] Kleefsman, K. M. T., Fekken, G., Veldman, A. E. P., Iwanowski, B., and Buchner, B., 2005. "A Volume-of-Fluid based simulation method for wave impact problems". *J. Comput. Phys.*, **206**, pp. 363393.

[13] Duz, B., Huijsmans, R.H.M., Wellens, P. R., Borsboom, M.J.A. and Veldman, A. E. P., 2011. "An absorbing boundary condition for regular and irregular wave simulations". In Proc. 5th Int. Conf. on Computational Methods in Marine Engineering MARINE2011.

[14] Kleefsman, K. M. T., 2005. "Water impact loading on offshore structures - a numerical study". PhD Thesis, University of Groningen, The Netherlands.

[15] Veldman, A. E. P., Gerrits, J., Luppes, R., Helder, J. A., and Vreeburg, J. P. B., 2007. "The numerical simulation of liquid sloshing on board spacecraft". *J. Comput. Phys.*, **224**, pp. 8299.

[16] Duz, B., Huijsmans, R.H.M., Wellens, P. R., Borsboom, M.J.A. and Veldman, A. E. P., 2011. "Towards a general-purpose open boundary condition for wave simulations". In Proc. 30th Int. Conf. on Ocean, Offshore and Arctic Engineering OMAE2011. Paper OMAE2011-49979

[17] Skjelbreia, L., Hendrickson, J. Fifth order gravity wave theory. *In Proc. 7th Conf. of Coastal Engineering* (1961) 184–196.